We are IntechOpen, the world's leading publisher of Open Access books Built by scientists, for scientists

6,900
Open access books available

186,000
International authors and editors

200M
Downloads

Our authors are among the

154
Countries delivered to

TOP 1%
most cited scientists

12.2%
Contributors from top 500 universities

WEB OF SCIENCE™

Selection of our books indexed in the Book Citation Index in Web of Science™ Core Collection (BKCI)

Interested in publishing with us?
Contact book.department@intechopen.com

Numbers displayed above are based on latest data collected.
For more information visit www.intechopen.com

3

Control of a 3KW Polar-Axis Solar Power Platform with Nonlinear Measurements

John T. Agee and Adisa A. Jimoh
Tshwane University of Technology, Pretoria, South Africa

1. Introduction

Environmental concerns and the finiteness of fossil fuels have engendered a global embrace for alternative energy systems. Botswana is a country blessed with abundant solar energy resources: having a mean solar day of 8.8 hours and 320 days of clear sunshine in a year (Anderson & Abkenari, 1999; Botswana Energy Report, 2003). It also experiences an excellent mean solar radiation intensity of 5.8/KW.m^2 (Anderson & Abkenari, 1999). Given that the country currently meets about 70% of her electricity needs through imports from the Southern African Power Pool (SAPP) (Botswana Power Corporation, 2004; SADC, 2004; Matenge & Masilo, 2004), the country is well motivated to integrate solar power into its energy generation base.

Earlier attempts at integrating solar power generation into the national energy mix in Botswana in the eighties, and, in fact, up to the nineties, advocated the use of solar power installations of a few Watts' capacity for lighting in small rural communities. Moreover, such solar power projects employed static installations. Static solar power installations generally have lower daily and seasonal efficiencies than sun-tracking installations. Compared to tracking systems, the lower efficiencies of static solar installations often mean that additional photovoltaic panels must be mounted to meet the required output capacity, thus raising the over-all cost of the facility. Consequently, the above-mentioned solar power philosophy imploded by reason of two shortcomings: customers' perception that initial installation costs were unduly high; and the sentiments of financial institutions that the business value of such small capacity installations was insignificant. Experiences around the SADC countries generally show that such integration philosophies have always not been sustainable (Geche & Irvine, 1996; Mogotsi, 2002; Lasschuit *et al*, 2009). For Botswana, as well as for several other countries in the SADC (Southern African Development Council) region, the high initial costs of solar power installations have been a major hindrance to the massive adoption of solar energy for rural communities (BPC, 2005; Solarie 2005).

The current development of solar power equipment for use in Botswana, and the possible subsequent extension to other SADC countries benefited from the findings reported above. First of all, the current efforts concentrate on the development of solar power equipment that could support rural entrepreneurial activities, in addition to basic lighting needs. This approach is rooted in the understanding that sustainability could be enhanced with the

Source: Solar Energy, Book edited by: Radu D. Rugescu,
ISBN 978-953-307-052-0, pp. 432, February 2010, INTECH, Croatia, downloaded from SCIYO.COM

stimulation of economic activities. This approach is also thought to be supported by the fact that rural individuals could be motivated to acquire solar power systems that might enhance their economic wellbeing; and also that, such solar power installations with added economic value would attract the support of local financial institutions. Tables 1 to 3 show examples of typical rural enterprises around Botswana, and the example power requirements (SADC Report, 2004; de Lazzer, 2005). Additional scenarios that could be considered include cold storage facilities for anti-retroviral drugs, rural guest houses for tourism, battery charging and welding businesses. In all studied cases, the power requirements could be considered to be in the range 1-3KW; this forming the basis for the 3KW rating of the solar power platform studies presented in the chapter. Secondly, the current approach for equipment development uses tracking solar power systems, as opposed to the earlier approach that utilized static solar power systems. An extensive discussion comparing tracking solar power systems is presented elsewhere (de Lazzer, 2005; Agee et al 2006a). Suffice it to state that, polar-axis tracking systems present an option capable of producing 97.5% the output power of two-axis solar power systems; and this at acquisition and maintenance costs similar to those of the cheaper single-axis installations. This comparative economic advantage informed our choice of the polar-axis tracking solar power systems for the study reported in this chapter.

For the rest of the chapter, the physical structure and the data of the solar platform system is presented in section two. Dynamic modelling of the platform and model studies is presented in section three. Sensor characteristics modelling and validation form the contents of section four. Two controllers are investigated for the enhancement of the dynamic performance of the polar-axis solar power platform. The design and comparative analysis and discussions of these controllers is presented in section five of the chapter. Section six contains the conclusions and recommendations for further research. A list of references is included in section seven, to conclude the chapter.

Equipment	Power Consumption (W)
Refrigerator with freezer	550
Lighting bulb 60W (x2)	120
Television 51cm color	80
Radio portable	6
Fan	250
TOTAL	**1006**

Table 1. Energy requirements of a rural bar

Equipment	Power Consumption (W)
4 computers	1200
light	60
Radio-cassette	6
TV color	80
TOTAL	**1346**

Table 2. Energy requirements of a rural internet café.

2. Description of the 3KW polar-axis solar tracker hardware

Ten, 300KW solar panels were required to realize the 3KW design power level. Thus, the platform carries ten Shott 300W solar panels. In addition, two smaller Shell SQ 80W solar panels are provided to compensate for the energy looses and the power required in the electrical drive system (Alternative Energy Store, 2005; Shell.com, 2005). The detailed design of the 3KW solar power platform is presented in (de Lazzer, 2005). The weight of each of the 300W solar panels is 46.6Kg. The weight of the 80W solar panel is 7.5Kg /panel. The total weight is ≈500 Kg. The platform is 7 meters long by 3.8 meters wide. Therefore, the area of the platform is 26.4m^2. For the 300W solar panels, the weight is distributed on all the frame perimeter. The concentrated force value is 0.1 N/mm. For the 80W solar panels, the weight is distributed on the frame length only and its value is 0.03 N/mm. The solar panels are fixed symmetrically with respect to the beams of the platform. It is assumed that the structure experiences no dynamic effects. The load can therefore be classified as static. The arrangement of solar panels is shown in Figure 1. The standing 3KW platform is shown in Figure 2. The drive system consist of a d.c motor linked to the platform through a gear train having a gear ratio of 800. Additional provision was made for manual control for the purposes of field experimentation in the Botswana environment. This manual provision for the seasonal adjustment of the longitudinal inclination of the platform is visible from Figure 2, where it appears as a knob on the stem supporting the platform.

Equipment	Power (W)
4 refrigerators with freeze	2100
3 lights	120
Hi Fi	180
2 TV 51cm color	160
TOTAL	**2560**

Table 3. Energy requirements for a rural clinic

Parameters and their values		
R_a=5Ω	L_a=0.003H	B=3.95.10^{-6} Kg.ms^{-1}
K_b=0.0636V/ rad/s	K_m=0.00711 Kgm/A	K=0.01Kg m^2/ s^2
J_M=7.72.10^{-6} Kg m^2	J_L=970Kgm^2	N=1/n=1 /800

Table 4. System parameters

The platform is a sensor-based tracking solar power platform. As suggested by the name, this type of tracking solar power system employs two photosensitive detectors to determine the position of the sun. Usually, two sensors are positioned on an imaginary line parallel to the east-west axis passing through the centre of the array of solar panels. They are arranged so that they produce a differential output whenever the active surface of the solar panels is not aligned perpendicular to the direction of sunrays. When the incident solar radiation is perpendicular to the plane of the array of PV cells, both sensors generate equal amount of

current. If however, the incident solar radiation is not perpendicular to the array, then one of the sensors produces an output current greater than that of the second sensor. The differential output current from the sensor arrangement is a current whose magnitude depends of the angle of misalignment of the panels. The sign of the resultant current indicates the direction of the sun. The control system utilises the output of the sensor arrangement to control the motor that rotates the platform of solar panels until the electrical signal in each of the light detectors becomes equal.

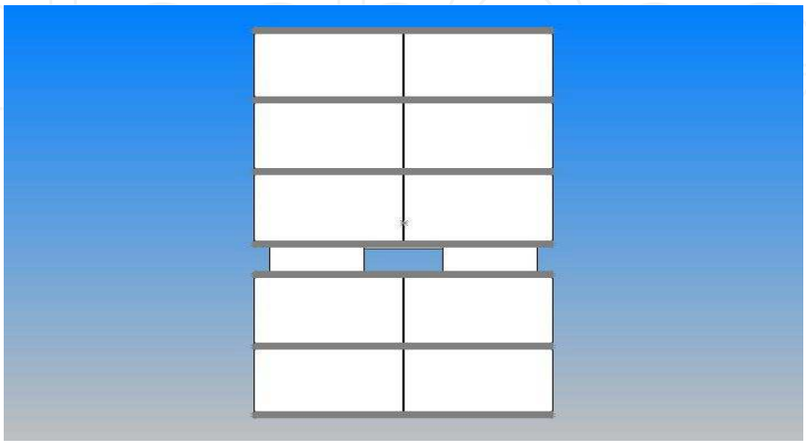

Fig. 1. Arrangement of solar panels on the platform.

For the purpose of investigating the dynamic performance of the platform, as well as for controller design , a model of the platform is developed, based on the application of relevant physical laws. The platform modeling is presented in the next section, section three of the chapter.

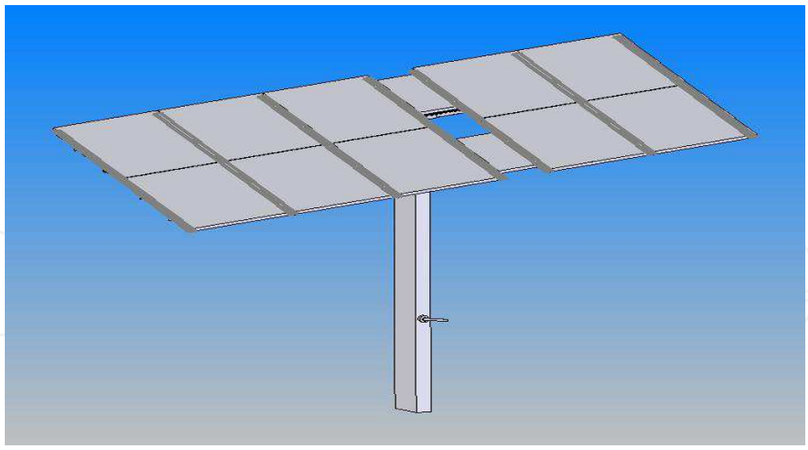

Fig. 2. The 3KW platform viewed from above

3. Mathematical modelling and analysis of the dynamics of the basic platform

The subsequent modeling presented in this section concerns the east-west motion of the platform. The block diagram representation of the platform in the east-west direction is shown in Figure 3.

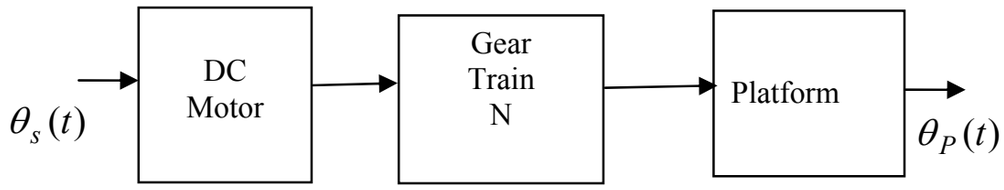

Fig. 3. Block diagram of 3KW solar power platform

Where: $\theta_s(t)$ is the instantaneous direction of sunlight and $\theta_p(t)$ the instantaneous position of the platform.

Hence, the model of the solar tracker is the system of dynamic equations linking the separately excited dc motor to the platform through the gear train as derived in the sequel.

3.1 Modelling of the separately excited DC motor

The typical equivalent circuit arrangement for a separately excited DC motor is shown in Figure 4. An applied armature voltage e_a creates an armature current i_a given by (Kuo & Golnaraghi, 2003):

$$e_a = R_a i_a + L_a \frac{di_a}{dt} + K_b \frac{d\theta_m}{dt} \tag{1}$$

where $e_a(t)$: armature voltage (V); $i_a(t)$: armature

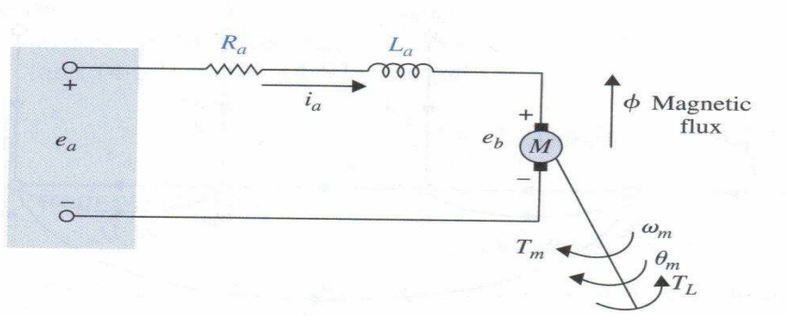

Fig. 4. Schematic diagram of a separately excited DC motor.

current (A); R_a: armature resistance (Ω); L_a: armature inductance (H); K_b: back-emf constant (V/rad/s) and $\theta_m(t)$: rotor displacement (rad.). This current causes a torque

$$T_m = K_m i_a \tag{2}$$

where $T_m(t)$ is torque(N.m.) and K_m the torque constant (N.m/A).

The torque of the DC motor is coupled to drive the platform through the motor shaft and a gear train. The torque causes an angular displacement of the rotor θ_m, given by (Kuo & Golnaraghi, 2003):

$$T_m = J_t \frac{d^2\theta_m}{dt^2} + B\frac{d\theta_m}{dt} + K\theta_m \tag{3}$$

where $J_t = J_m + N^2 J_l$ and J_m: moment of inertia of the motor ($kg.m^2$); J_l: moment of inertia of the solar power platform ($kg.m^2$); N: gear-train ratio between motor and platform; B: viscous-friction coefficient of the motor ($kg.m.s^{-1}$); K: spring constant ($kg.m^2.s^{-2}$). After taking the Laplace transform of equations (1)-(3), it is straightforward to obtain the open-loop transfer function for the system G(s)=θ_m/V_a as shown in equation (4).

$$G(s) = \frac{K_m / L_a J}{s^3 + \left\{\frac{R_a J_t + L_a B}{L_a J_t}\right\} s^2 + \left\{\frac{R_a B + K L_a + K_b K_m}{L_a J_t}\right\} s + \frac{R_a K}{L_a J_t}} \tag{4}$$

Note further that, the angular position of the platform θ_p is related to the motor angular position θ_m through the gear ratio:

$$\theta_p / \theta_m = N = 1/800 \tag{5}$$

The gear ratio was decided by comparing similar applications (Kuo & Golnaraghi, 2003).
The parameters of the open-loop platform system are given in the Table 4. A substitution of these parameters in equation (4) results in the open-loop transfer function:

$$G(s) = \frac{1559.2}{s^3 + 1666.7s^2 + 109.87s + 10965} = \frac{b}{s^3 + a_3 s^2 + a_2 s + a_1} \tag{6}$$

In subsection 3.2, the dynamic behaviour of this open loop system was investigated with the view to determining what controller would be most suitable for improving the platform dynamic performance.

3.2 Simulation of the open-loop platform system

The analysis of the dynamic performance of the platform was simulated using MATLAB. The following simulations were carried out.

3.2.1 Time-domain characterisation of the open-loop platform system

The system was simulated for a unit step increase in the input voltage. The results are shown in Figure 5. The performance of the system, from Figure 5, could be summarized as in Table 5. ***Settling Time*****:** It is evident from Figure 5 and the summary in Table 5 that the settling time of 105 seconds for the platform well exceeds one minute. This is too long and would not be suitable for the successful tracking of sunlight, since the direction of the sun rays is likely to change significantly before the platform settles down to the last command. Improvements in the settling time would be required. The peak overshoot is 96% of the final value. This is much higher than the maximum 17% overshoot acceptable in literature (Kuo & Golnaragh, 2003). The maximum overshoot must be reduced. For a third order system, the damping ratio is not strictly defined (Kuo & Golnaraghi, 2003). However, the contribution of the root s_3=-1670 in the transient response is negligible. The complex pole-pair s_1, s_2=-0.031±j2.56 are the significant poles of the system. Their damping factor ξ is equal to 0.0121. This is much less than the damping factor of ≈ 0.707 required for optimum plant performance (Norman, 2004). An appropriate control strategy should enhance the damping of the system.

Settling time	105 Sec.
Peak overshoot	96%
Steady state error	0.875%
Eigenvalues	-1670, -0.031±j2.56
Damping factor	0.0121

Table 5. Summary of the dynamic performance of the platform

Steady State Error: The steady state error of 0.875% is well less than the typical tolerance band values of either 2% or 5% and does not need any further improvement.

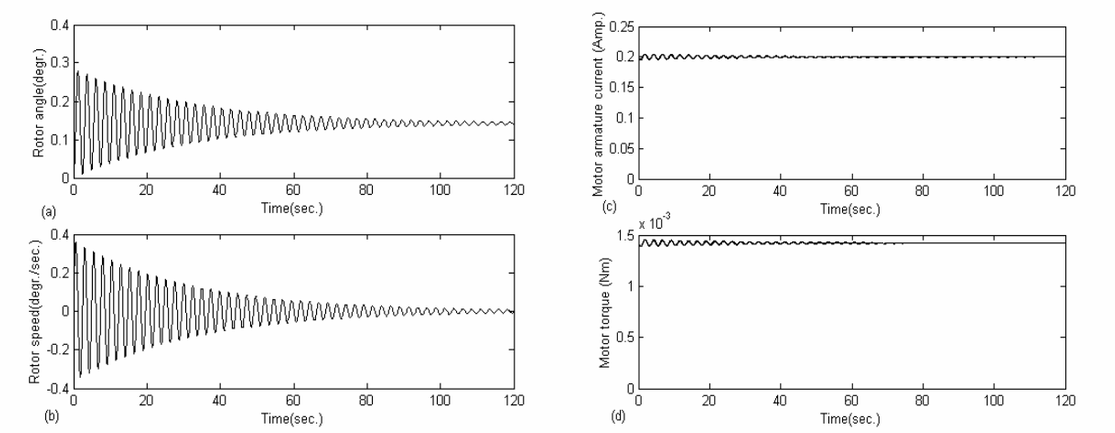

Fig. 5. Dynamic response of solar platform without feedback control

3.2.2 Frequency analysis of the open loop system

The frequency response of the open system is shown in Figure 6. From the Bode plot, the Gain and Phase margins are read. The Gain margin is 40.86dB and the phase margin is 10.4 deg. While the gain margin seems adequate, the phase margin is too low; and is hence due

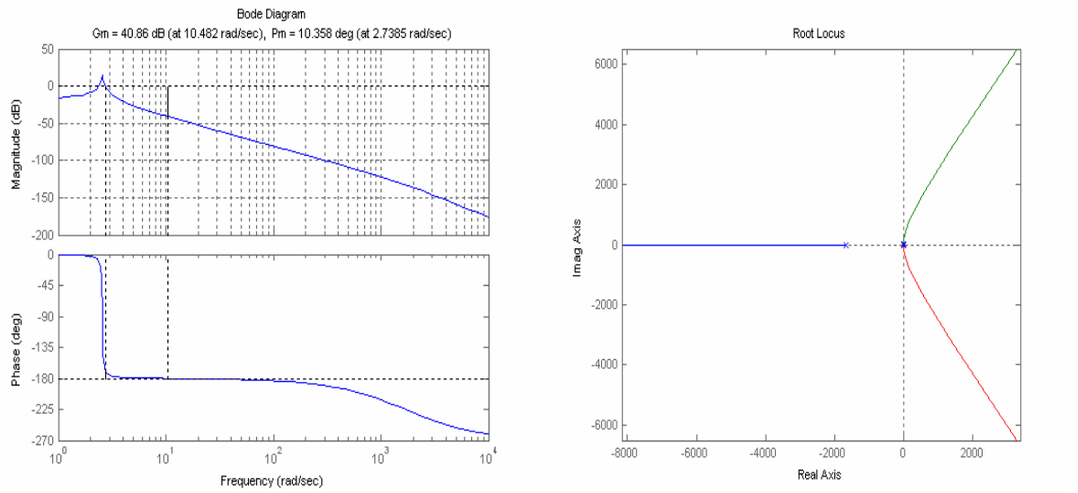

(a) (b)

Fig. 6. (a) Bode plot of open- loop platform (b) The root locus of open-loop platform

for further improvements. More over, the roots-locus plots (Figure 6.b) show that even for very small increases in the forward gain of the system, the dominant pole pair crosses the imaginary axis into the right half of the s-plane. It could be concluded that a control strategy that only increases the forward gain of the system, such as proportional control, would aid instability. In the next section of the paper, we present the design of a controller that avoids increases in the forward gain of the system; and which replaces the existing dominant pole-pair of the plant with ones that have the optimum damping factor.

3.3 Summary results from dynamic simulations of the basic platform system

The open-loop simulations of the platform model show that the steady state error of the open-loop dynamics is satisfactory, hence needs no further improvements. The settling time of 105 seconds is well in excess of practical requirements for such systems; and needs to be substantially reduced. The controller design shall specify a target settling time of 2 seconds. The settling time of the open-loop platform system is, in fact, due to the poor damping factor ξ= 0.0121. Alternatively, the poor settling time could be interpreted as a consequence of the dominant pole-pair s_1, s_2=-0.031±j2.56 existing close to the origin of the ***s***-plane. It therefore seems plausible to explore the use of a controller or controller-types that will cancel the existing dominant pole-pair and replace them with those that optimise the damping of the platform. Linear systems are considered to be optimally damped if the damping factor $\xi \approx 1/\sqrt{2}$ (Kuo & Golnaragh, 2003).

4. Sensor modelling and characterisation

For the purpose of effecting feedback control of the platform, a sensor required to measure the relative orientation of the platform axis $\theta_p(t)$ for feedback was required. As indicated in section two of the chapter, a photovoltaic position sensor was employed for the measurement of the misalignment α(t) between the orientation of the platform axis and the direction of sun rays. Hence the sensor measurements are a function of the variable $\alpha(t) = \theta_s - \theta_p(t)$. The sensor consists of two photocells. The derivation of the sensor output relationship begins with a recollection of the theory of the photovoltaic cell.

4.1 The photovoltaic cell

The photovoltaic cell is a two terminal device which consists of a photodiode. The photodiode may be a p-n junction or p-i-n structure. When the cell absorbs light, mobile electrons and positively charged holes are created. If the absorption occurs within the junction's depletion region, or one diffusion length away from it, these carriers are swept from the junction by the built-in field of the depletion region, producing a photocurrent (Nelson, 2003). A detailed representation of the current phenomenon in a photocell, accounting for internal diode current is given as:

$$i_0 = I_{PH} - I_D = I_{PH} - I_S \cdot \{\exp(V / mV_T) - 1\}. \quad (7)$$

Where: I_{PH}: Photo current; I_D: Diode current; I_S: Diode reverse saturation current; m: Diode "ideally factor" m= 1-5V_T; Thermal voltage: $V_T = kT / e$; k: constant of Boltzmann; T: absolute temperature; *e:* charge of an electron. Internal voltage drop in practical photocells

is accounted for by the addition of a series resistor R_S. Also leakage currents could be observed in photocells, which may be described as due to a parallel resistor R_p ; from these we could write the photocurrent of the photocell as:

$$0 = I_{PH} - I_D - I_P - i_0 \tag{8}$$

And

$$I_P = \frac{V_D}{R_P} = \frac{V + i_0 R_S}{R_P} \tag{9}$$

Hence,

$$i_0 = I_{PH} - I_S \left\{ \exp\left(\frac{V + i_0 R_S}{m V_T} \right) - 1 \right\} - \frac{V + i_0 R_S}{R_P} \tag{10}$$

4.2 The photovoltaic position sensor

Two photovoltaic cells were required to measure the position of the solar power platform, relative to the axis of sunlight. A photocell each was installed on either side of a line running perpendicular to the direction of rotation of the platform. Let these cells be "A" and "B" respectively, as shown in Fig. 7. The opening of the enclosure has a width of *W*. Each cell has the breadth *D* and height *C*. The cells are located a distance *L* behind the opening. Each cell generates a current, I_A and I_B, respectively, proportional to the intensity of its incident radiation. The difference between I_A and I_B is conditioned to generate an error voltage which could then be used to control the motion of the platform, as explained in the next subsection (Kuo & Golnaragh, 2003). It shall be shown below, the relationship between the cell currents I_A, I_B, and angle of misalignment α, of the platform.

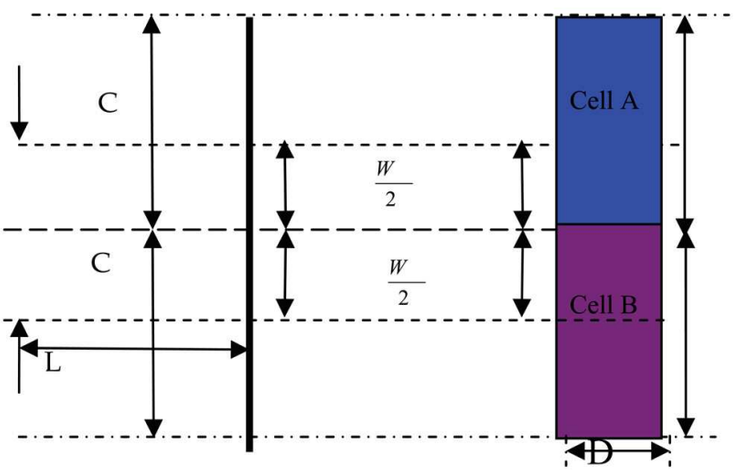

Fig. 7. Arrangement of photocells in the photovoltaic position sensor

4.3 Relating the light-intensity, exposed area of the cell and cell photocurrent

Consider the ray geometry of the photovoltaic position sensor with two identical photocells as shown in Fig. 8. With light incident perpendicular to both cells (angle of misalignment α=0), the area of each cell, exposed, is given by

$$A_A = A_B = (W/2) * D \tag{11}$$

Both cells intercept the same amount of incident radiation, producing the same amount of current. In such a case, the difference between the two current values is zero and no error signal is produced. Now, consider the situation in which an angular misalignment of $\alpha \neq 0^0$, causes the incident light to enter the enclosure of the sensor at an angle of inclination α to the axis of the two cells. Then, from Fig. 8, the exposed areas of cells A and B are respectively given by:

$$A_A = D(\frac{W}{2} + h); A_B = D(\frac{W}{2} - h) \tag{12}$$

Also, from the geometry in Fig. 8,

$$h = L\tan\alpha \therefore A_A = D(\frac{W}{2} + L\tan\alpha); A_B = D(\frac{W}{2} - L\tan\alpha) \tag{13}$$

With the intercepted light energy being proportional to the light-sensing surface area of the intercepting cell,

$$P_{RA} = I_R D(\frac{W}{2} + L\tan\alpha); P_{RB} = I_R D(\frac{W}{2} - L\tan\alpha) \tag{14}$$

The photocurrent I_{PH} of a cell is known to be proportional to the light energy, therefore:

$$I_0 \propto P_R \tag{15}$$

Therefore, from Eq. (14), and Eq. (15), one can write:

$$\begin{aligned} i_A &= K_1 P_{RA} = K_1 I_R D(\frac{W}{2} + L\tan\alpha); \\ i_B &= K_1 P_{RB} = K_1 I_R D(\frac{W}{2} - L\tan\alpha) \end{aligned} \tag{16}$$

Substituting Eq. (16) into Eq. (10) yields:

$$\begin{aligned} i_A = K_1 I_R D\frac{W}{2} + K_1 I_R DL\tan\alpha - I_S(e^{\frac{V_O \log(1+I_R)}{mV_T}} - 1) \\ - \frac{V_O \log(1+I_R) + I_A R_S}{R_P} \end{aligned} \tag{17}$$

and,

$$\begin{aligned} i_B = K_1 I_R D\frac{W}{2} - K_1 I_R DL\tan\alpha - I_S(e^{\frac{V_O \log(1+I_R)}{mV_T}} - 1) \\ - \frac{V_O \log(1+I_R) + I_B R_S}{R_P} \end{aligned} \tag{18}$$

Now, the differential output current for the cells would now be approximated as:

$$i_A - i_B = 2K_1 I_R DL\tan(\theta_s - \theta_p) \tag{19}$$

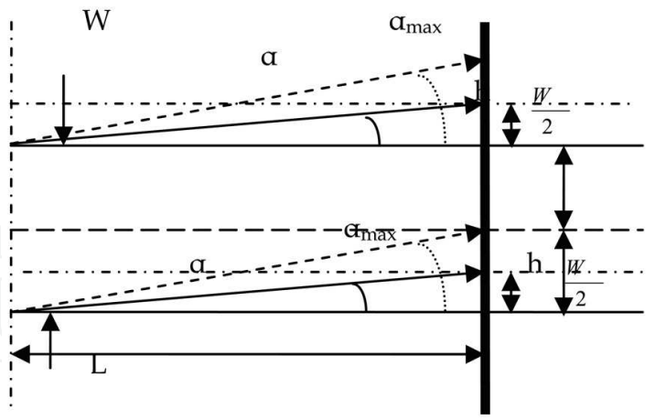

Fig. 8. Ray geometry in the sensor

4.4 The feedback signal

The circuit for feedback signal generation is shown in Figure 9. As derived in (Agee *et al*, 2009), the resultant output current, representing the difference between the direction of the sun rays θ_s and the axis of the rotor θ_m is given by (20):

$$i_A - i_B = 2K_1 I_R DLan(\theta_S - \theta_P) \tag{20}$$

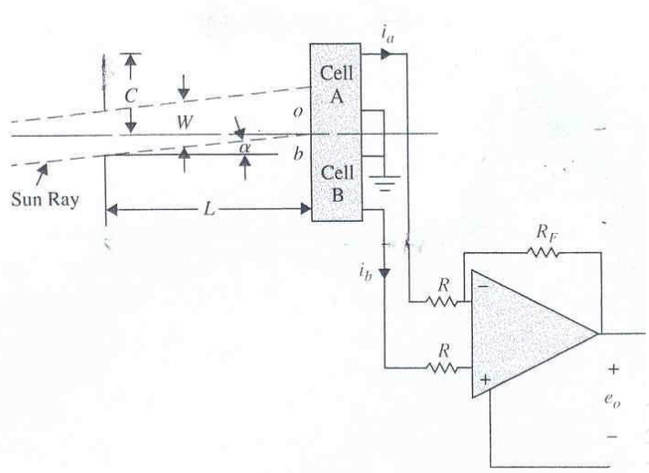

Fig. 9. Sensor signal conditioning for feedback

where i_A, i_B are cell currents from cells A and B respectively. The error voltage signal e_o is straight away derived from Figure 9, to be:

$$e_o = -R_F(i_A - i_B) = -2K_1 I_R DLR_F \tan(\theta_S - \theta_P) \tag{21}$$

However, with the introduction of a unity-gain inverting amplifier in the follow-up stage, we have

$$e_{o1} = -e_o = R_F(i_A - i_B) = 2K_1 I_R DLR_F \tan(\theta_S - \theta_P) \tag{22}$$

Thus with the measurements included for feedback control, the armature voltage V_a could now be expressed as

$$V_a = K_F(e_{o1}) = 2K_F K_1 I_R DLR_F \tan\alpha; \qquad \alpha = \theta_S - \theta_P \tag{23}$$

where, K_F is a constant of proportionality. For linear controller design, a linearised representation of sensor characteristics is required. By approximating $\tan(\theta_S - \theta_P) \cong \theta_S - \theta_P$, the linear sensor feedback model takes the form:

$$V_a = K_F(e_{o1}) = 2K_F K_1 I_R DLR_F \alpha \tag{24}$$

4.5 Validation of sensor model

The data in Table 6, together with equations (17) and (18) were used for the numerical validation of sensor model. Simulations were done in MATLAB. Fig. 10 and Fig. 11, respectively, confirm the nonlinear relationships between I_A, I_B and α. Figure 12 show the nonlinear relationship between α and the differential output cutrrent of the sensor.

PARAMETER	VALUE	PARAMETER	VALUE
Light intensity I_R	12 [mW/cm²]	R_S	5 [Ω]
Sensitivity of sensor K_1	0.55 [AW^{-1}]	D	5 [cm]
m, the ideal diodes factor	1	L	0.8 [cm]
Temperature voltage V_T	25.7 [mV] at T = 25°C	W	3.5 [cm]
Reverse saturation current	I_S = 2x10^{-6}[A]	C	5 [cm]
Photo-voltage V_O	0.5 [V]	Area	12.5 [cm²]
Parallel resistance R_P	1 [KΩ]		

Table 6. Data used for the simulation of the photovoltaic position sensor

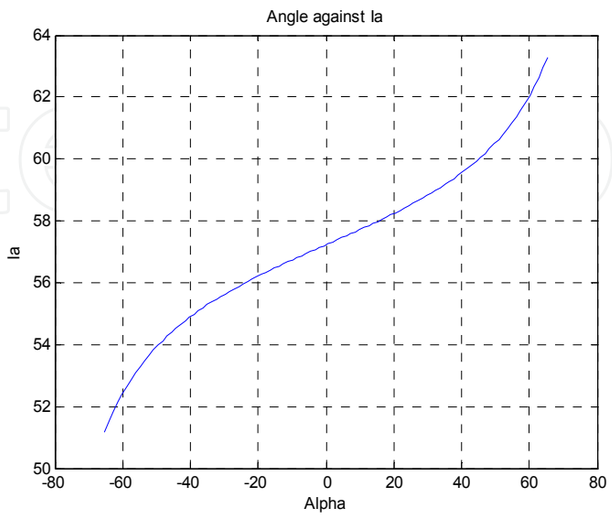

Fig. 10. Current I_A versus angle α

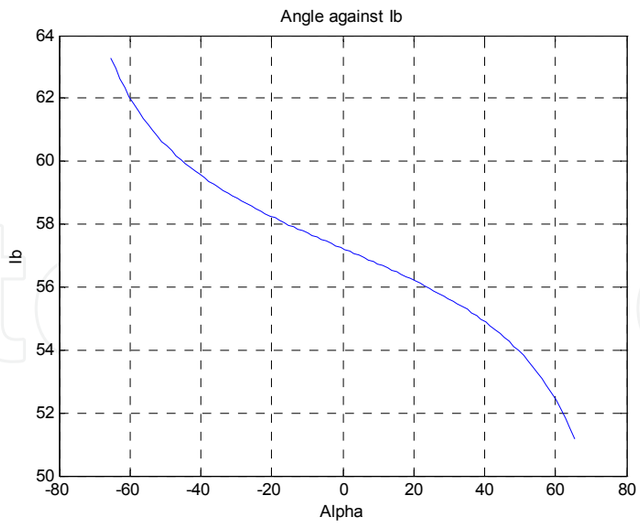

Fig. 11. Current I_B versus angle α

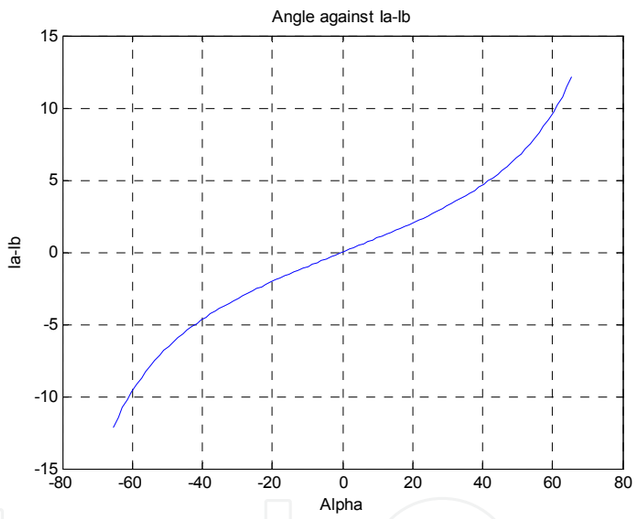

Fig. 12. $I_A - I_B$ related with angle α.

5. Controller design

The structure for the platform system with controller is shown in Figure 13. This shows the embedding of the photosensor into the feedback network.

5.1 Performance specification

The controller was required to modify the response of the system in such a manner as to achieve the following performance specification:

- Settling time for 2% tolerance band = 2 seconds.
- Damping factor = 0.71

First, the pole-cancellation controller is designed and validated. A critical appraisal of the performance of the controller in the presence parameter variations and nonlinearities is

presented. Finally, the design of the nonlinear controller, and a comparative analysis of its performance with respect to the pole-cancellation controller are presented.

5.2 Design of the pole cancellation controller for the platform

The structure for the system with controller is shown in Figure 13. The Figure shows the position of the sensor presented in section (4) of the chapter. It has been explained earlier that, both the settling time and the damping of the platform system need improvement. Our solution was to use a controller whose transfer function zeros cancelled the undesirable poles of the platform transfer function, G(s). Then, the poles of the controller were placed so as to achieve the desired closed-loop dynamic performance. Accordingly, the structure of the controller is specified to be the notch filter with the following transfer function:

$$G_C(s) = \frac{K_1 s^2 + \alpha_1 s + \beta_1}{K_2 s^2 + \alpha_2 s + \beta_2} = \frac{N_1(s)}{D_1(s)} \tag{25}$$

as shown in Figure 14 (Agee *et a*l, 2006).

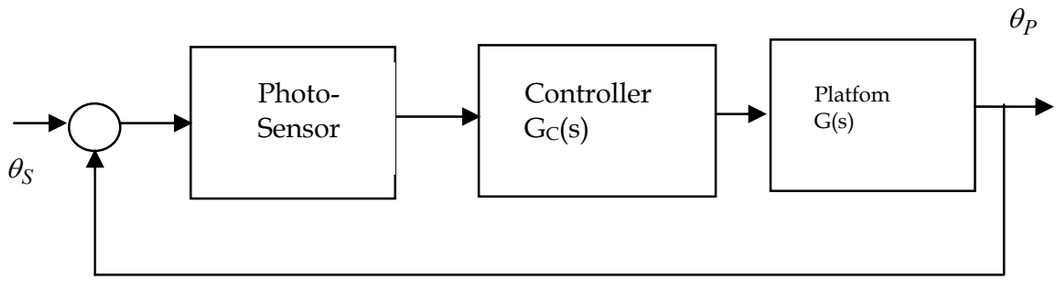

Fig. 13. Block diagram of controlled platform

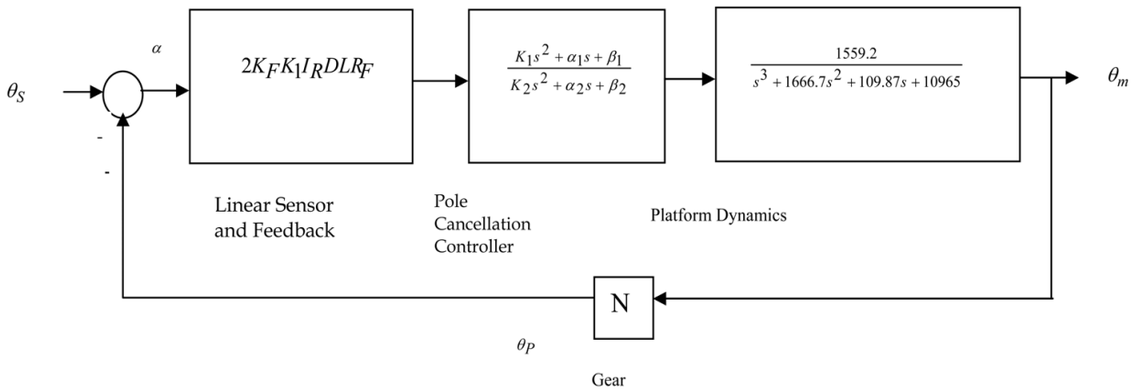

Fig. 14. Closed-loop block diagram of platform with a linear sensor

5.2.1 Tuning of pole-cancellation controller

The controller design entails the determination of the six coefficients K_1, α_1, β_1, K_2, α_2 and β_2. Note that the zeros of the controller are required to cancel the dominant pole-pair of the

open-loop transfer function of the platform system. With the pole-cancellation controller included as in Figure 14, the closed-loop transfer function of the platform becomes equation (25). To determine K_1 , α_1 and β_1 for the controller, consider the closed loop transfer function for the controlled system with linear sensor characteristics. Then, using the fact that the dominant pole-pair of the open loop transfer function is : -0.031±j2.56;

$$C(s) = \frac{(2K_F K_1 I_R DLNR_F G_C(s)G(s)}{1 + (2K_F K_1 I_R DLNR_F)G_C(s)G(s)} \tag{26}$$

An equivalent second-order polynomial for the zeros of the notch filter is obtained. Hence, K_1 = 1; α_1 =0.062 and β_1 =6.5546. Now, let $2K_F K_1 I_R DL = 1$, such that,

$$G_C(s)G(s) = \frac{(s + 0.031 - 2.56j)(s + 0.031 + 2.56j).1559.2}{D_1(s)(s + 1670)(s + 0.031 - 2.56j)(s + 0.031 + 2.56j)}$$

or,

$$G_C(s)G(s) = \frac{1559.2}{(K_2 s^2 + \alpha_2 s + \beta_2).(s + 1670)}$$

Then, for the closed-loop platform with pole-cancellation,

$$C(s) = \frac{1559.2NR_F}{(K_2 s^2 + \alpha_2 s + \beta_2).(s + 1670) + 1559.2NR_F} \tag{27}$$

$$C(s) = \frac{1559.2NR_F / K_2}{s^3 + (\frac{\alpha_2}{K_2} + 1670).s^2 + (\frac{\beta_2}{K_2} + 1670\frac{\alpha_2}{\beta_2})s + (1670\frac{\beta_2}{K_2} + 1559.2\frac{NR_F}{K_2})} \tag{28}$$

Also, for a damping factor of 0.71, the settling time is given by: $t_{s_{1\%}} = 4.6 / \xi\omega_n$ (Kuo & Golnaraghi, 2003). Thus, for a settling time of 2 seconds, we deduce ω_n = 3.24 rad/s. The new dominant pole-pair is given by $s_{1,2} = -\xi\omega_n \pm \omega_n\sqrt{1-\xi^2}$, yielding the dominant second-order factor $s^2 + 2\xi\omega_n + \omega_n{}^2$. With the third-pole of the closed-loop system situated at s= -d, we have the characteristic equation of the controlled system to be

$$s^3 + (d + 2\xi\omega_n)s^2 + (\omega_n^2 + 2\xi\omega_n d)s + d\omega_n^2 = 0 \tag{29}$$

Compare equations (28) and (29) to obtain the following relations:

$$\begin{aligned} 160y + z &= d\omega_n^2 \\ \omega_n^2 + 2\xi\omega_n d &= y + 1670x \\ d + 2\xi\omega_n &= 1670 + x \end{aligned} \tag{30}$$

Where,

$$x = \frac{\alpha_2}{K_2}, z = \frac{1.949 R_F}{K_2}; y = \frac{\beta_2}{K_2} \tag{31}$$

The simultaneous solution of equation (30) yields:

$$\begin{aligned} \omega_n &= 1670\xi \pm \sqrt{697225\xi^2 - 2788900 + z/\Delta} \\ \Delta &= d - 1670 \end{aligned} \tag{32}$$

It becomes a matter of substitutions to verify that for the given settling time of 2 seconds and damping factor $\xi = 0.71$, equation (32) is satisfied for

$$z = 2893.664, \Delta = 0.0001 \tag{33}$$

and further that the closed loop pole d=-1670.0001, $\alpha_2 / K_2 = 4.6008; \beta_2 / K_2 = 8.7648$. By setting K_2=1, obtain the complete transfer function of the controller as:

$$G_C(s) = \frac{s^2 + 0.0620s + 6.5546}{s^2 + 4.6008s + 8.7648} \tag{34}$$

and $R_F = z / 1.949 = 1.485K\Omega$

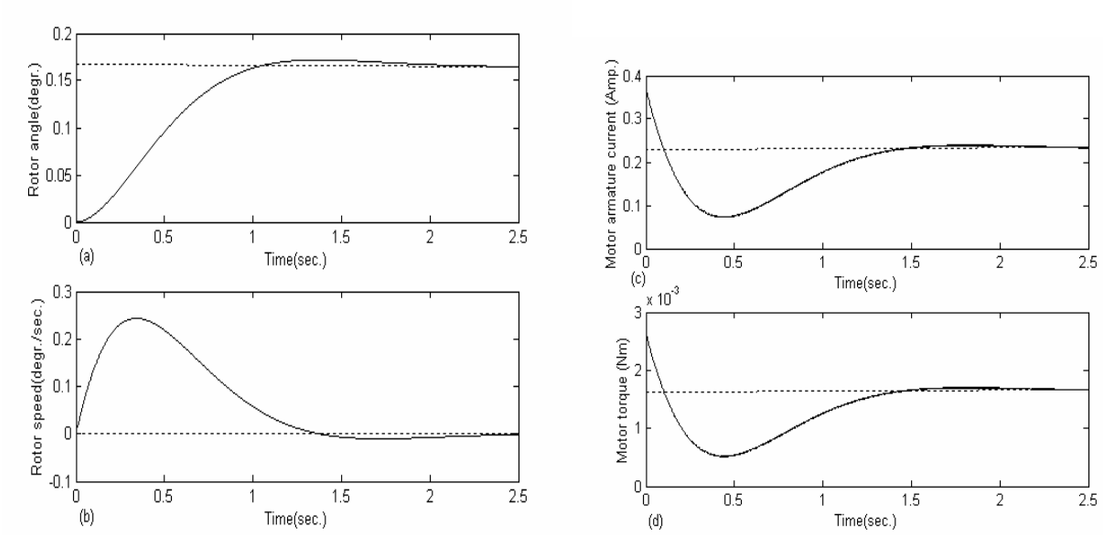

Fig. 15. Analysis of platform system controlled by pole-cancellation

5.3 Performance of the platform equipped with pole-cancellation controller

The transfer function of the closed-loop system with controller becomes:

$$C(s) = \frac{1665855}{s^3 + 1674s^2 + 7688s + 17505} \tag{35}$$

Both the transient response and the frequency response of the controlled system were simulated. The results are shown in Figure 15. It can be seen that, with the controller included, the system does not oscillate like it did before the introduction of the controller.

The overshoot is 4.3%. Overshoot peak has been reduced by 95%, as compared to the case of the uncontrolled system. The damping factor is improved to 0.71. The settling time is now reduced to 2 seconds. The steady state error is only 0.01 rads. This is much better than for the uncontrolled system. In fact, the steady state error has been reduced by 99%. The system is stable. The gain margin is improved by 75% to about 73dB while the phase margin is now infinity. The peak armature current has been reduced by 25% from 0.2A to 0 0.16 A. The peak torque required in the drive system increased from 1.5mN.m to 2.7mNm. It could therefore be concluded that the pole cancellation control strategy improved significantly the dynamic performance of the 3KW solar power platform; improving the damping factor from 0.0121 to 0.71; reducing the settling time from 105 sec. to 2 sec. Peak overshoot of the rotor angular position was reduced by 95%. Both the gain margin and the phase margin were also substantially improved. The peak torque requirement however was doubled. The controller structure is simple and may be easily implemented. However, the design neglected nonlinear sensor characteristics which may restrict the usefulness of the control strategy presented here. These effects on the performance of the pole-cancellation controller are discussed in details in subsection (5.4).

5.4 A Critical analysis of the shortcomings of the pole-cancellation control strategy for platform control

In practical systems, the efficacy of the pole-cancellation control strategy is limited by the effects of parameter variation/uncertainty and the nonlinear sensor behaviour. These two effects are discussed further in the following two subsections.

5.4.1 Effect of parameter uncertainty on performance of platform controlled by pole cancellation

Consider the effect of additive parameter change on the open-loop platform model of equation (6). The resulting platform representation will admit the form in equation (36). Hence,

$$G(s)+\Delta G(s)=\frac{b+\Delta b}{s^3+(a_3+\Delta a_3)s^2+(a_2+\Delta a_2)s+(a_1+\Delta a_1)} \tag{36}$$

Or, more specifically:

$$G(s)+\Delta G(s)=\frac{1559.2+\Delta b}{s^3+(1666.7+\Delta a_3)s^2+(109.87+\Delta a_2)s+(10965+\Delta a_1)} \tag{37}$$

Numerical investigation of the platform systems with variable parameters in MATLAB yielded the roots variations shown in Table 7. It is evident from Table 7 that the open-loop poles of the platform change significantly with variation in system parameters. Under such circumatances, a basic pole-cancellation control strategy will be ineffective, except where on-line adaption is introduced. Such additional complexities in the structure of the controller would make the above control strategy more expensive and hence, less attractive.

Moreover, the increased complexity in the systems would lead to the more complex platform block diagram shown in Figure 16, with uncancelled dynamics, where:

Parameter	Variation	s_1	s_2	s_3
Δa_3	+5%	-1750	-0.035+2.5i	-0.035–2.5i
Δa_3	+10%	-1833.3	-0.036+2.4i	-0.036–2.4i
Δa_2	+5%	-1670	-0.037+2.6i	-0.037–2.6i
Δa_2	+10%	-1670	-0.040+2.6i	-0.040–2.6i
Δa_1	+5%	-1670	-0.039+ 2.6i	-0.039–2.6i
Δa_1	+10%	-1670	-0.041 +2.7i	-0.041-2.7i

Table 7. Dependence of platform system poles on parameter variation

$$\eta(s)=\frac{\left\{s^3+(1667.7+\Delta a_3)s^2+(109.87+\Delta a_2)s+(10965+\Delta a_1)\right\}\left\{s^3+1666.75s^2+109.87s+10965\right\}}{\Delta b\left(s^3+1666.75s^2+109.87s+10965\right)-1559.2\left(s^2+\Delta a_2 s+\Delta a_1\right)} \quad (38)$$

This, in turn, will modify the closed-loop response as shown in Figure 17-18. Note from Figure 17.b, that with a 10% increase in a_3, a non-positive defenite beahiour of the closed-loop platform is indicated. Figure 18 shows that, under some variations in a_2, the pole-cancellation controller loses function in steady state, and sustained oscillation of the plant is produced.

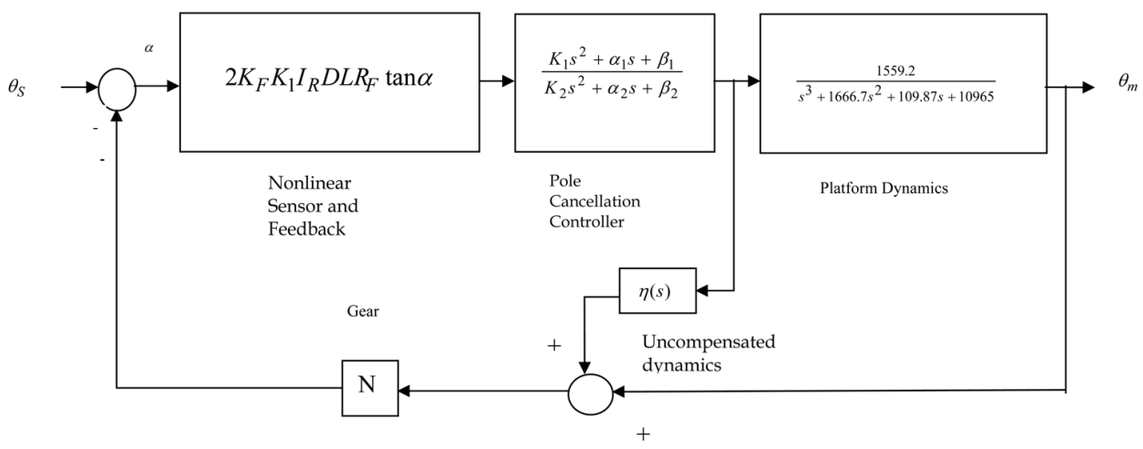

Fig. 16. Complex block diagram of platform due to failure of pole-cancellation

5.4.2 Effect of nonlinear measurement on linear controller performance

Recall that, while the approximate sensor characteristics was used for the design of the pole-cacellation controller, exact sensor characteristics are nonlinear, as in equation (23). In this subsection, a few comments are made as to how the true sensor characteristics affect the dynamics of the platform under pole-cancellation control.

Figure 19 compares the exact tangent characteristics with the linear approximation $\tan\alpha \approx \alpha$; together with the third-order polynomial approximation, $\tan\alpha \approx \alpha + \alpha/3!$. It is evident that none of the approximate representation is useful beyond $\alpha \geq 26^o$. Hence, the linear model is only valid within a very narrow window of the complete domain of operation of the solar power opearation. This will lead to significant model mismatches, for which the performance of the pole-cancellation controlle would be significantly inadequate.

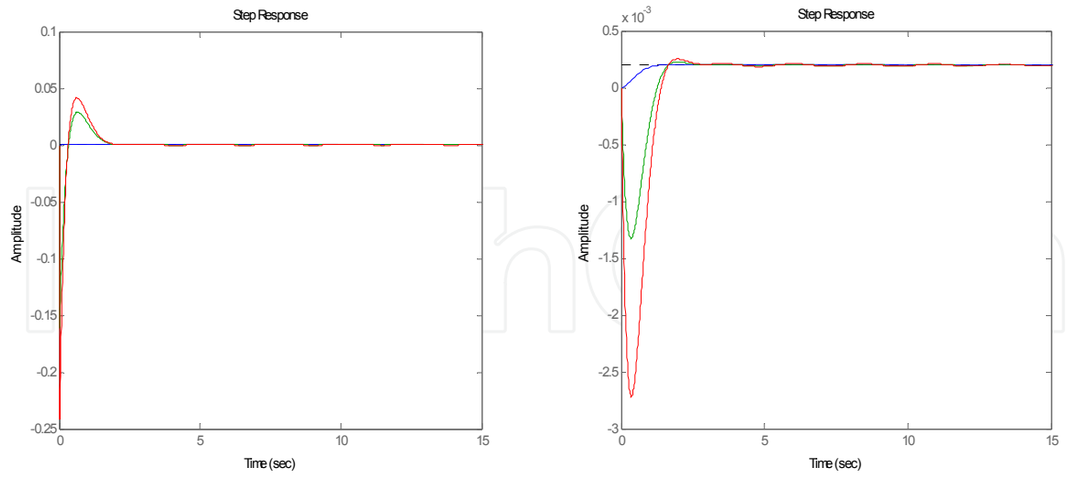

(a) (b)

Fig. 17. (a) Step response with a 5% variation of a_3 (b) Step response with 10% variation of a_3.

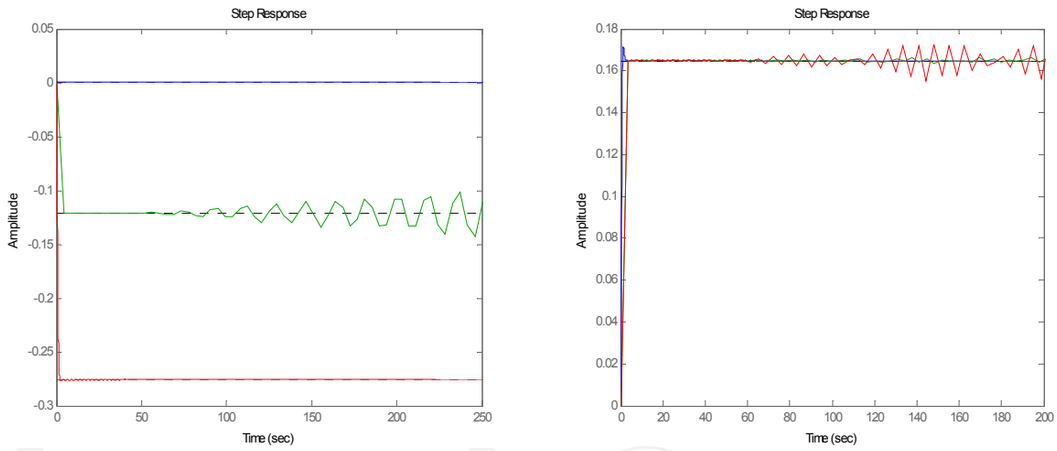

(a) (b)

Fig. 18. (a) Step response with 5% increase in a_2 (b) Step response with 10% increase in a_2

5.4.3 A summary perspective on the linear control of solar power platform

It is evident from the critical analysis of the effect of parameter variations and nonlinearity, that the suitability of linear control strategies for the polar-axis solar power platform with nonlinearities is limited. In particular, whereas the structure of the pole-cancellation controller makes controller implementation simple, the viablility of this strategy in the practical environments of parameter variation and nonlinearities is not guaranteed. Because of the very high forward gains of the platform, linear control was also not robust. On the other hand, the linear controlled system offers a suitable reference model for the comparison of the performance of possible nonlinear control strategies that may be employed on the platform system. In the rest of the chapter, the design and simulation of a nonlinear controller, the feedback-linearised control of the platform, is presented. Results are compared with those from the linear systems as presented above.

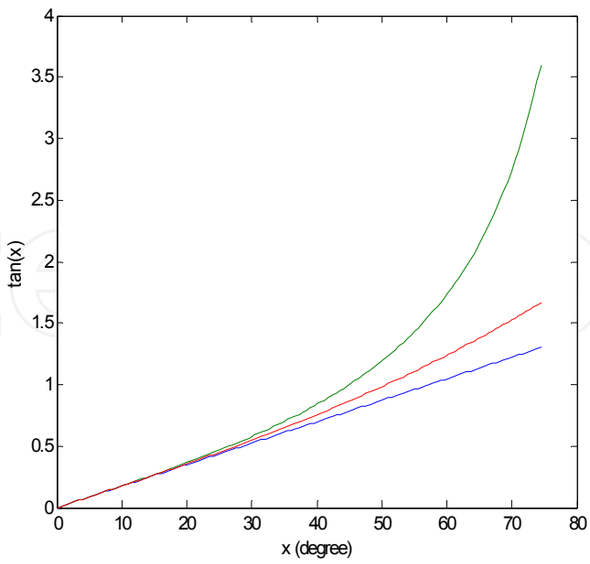

Fig. 19. Approximations of sensor tangent characteristics

5.5 Nonlinear control of platform

Feedback measurements used for the control of the tracking system lead to an overall nonlinear behaviour in the platform. This resulting nonlinear dynamics is much richer in complexity than the dynamics of the linear platform system. Consequently, nonlinear control strategies may be required to optimize the dynamic performance of the platform. The design of the nonlinear controller for the platform is presented in this section of the chapter. Controller discussions make comparisons of the nonlinear controller with the pole cancellation controller earlier designed for the tracking system.

5.5.1 The state space model of open-loop solar platform

Combining (1)-(3), it is straightforward to obtain the state-space representation for the open-loop systems, as shown in (39). Notice from the equation that, the basic open loop-loop platform, without feedback measurements is here again confirmed to be linear.

$$\begin{aligned} \dot{\theta}_1 &= \theta_2 \\ \dot{\theta}_2 &= \theta_3 \\ \dot{\theta}_3 &= -a_1\theta_1 - a_2\theta_2 - a_3\theta_3 + bV_a \\ y &= \theta_1 = \theta_m \end{aligned} \tag{39}$$

where,

$$a_1 = \frac{KR_a}{L_aJ_t}, a_2 = \frac{KL_a + BR_a + K_bK_m}{L_aJ_t}, a_3 = \frac{BL_a + J_tR_a}{L_aJ_t}, b = \frac{K_m}{L_aJ_t} \tag{40}$$

and $\theta = [\theta_1, \theta_2, \theta_3]^T \subset \Re^3 = [\theta_m, \dot{\theta}_m, \ddot{\theta}_m]^T$.

5.5.2 Nonlinear state-space model of platform with feedback measurements

The over all plant model, including the feedback measurement, will modify (39) to yield (41):

$$\begin{aligned}\dot{\theta}_1 &= \theta_2 \\ \dot{\theta}_2 &= \theta_3 \\ \dot{\theta}_3 &= -a_1\theta_1 - a_2\theta_2 - a_3\theta_3 + 2bK_FK_1I_RDLR_F\tan(\theta_s - \theta_m))\end{aligned} \tag{41}$$

It is thus evident from (35) that where as the basic system has a linear model, the measurements used for control make the overall system nonlinear

5.5.3 The non-linear input-state feedback control of polar-axis solar power platform

For the linearisation of the platform systems using feedback, a function of state $x_1 = \psi(\theta_1, \theta_2, \theta_3)$ is required; where the $r \le n$ derivatives of x_1 exist; and ψ is invertible such that all states of the platform $\theta_i; i = 1,2,..r$ and its input are functions of x_1 and its r derivatives. Recollect the fact that, for linear systems expressible in the controllable canonical form (as in equation (39), the input-state feedback linearising variable x_1 is the output of the canonical plant representation (Kuo & Golnaragh, 2003). It is possible to write that:

$$\begin{aligned}\theta_1 &= x_1 \\ \theta_2 &= \dot{x}_1 \\ \theta_3 &= \ddot{x}_1 \\ V_a &= (1/b)(\dddot{x}_1 + a_3\ddot{x}_1 + a_2\dot{x}_1 + a_1x_1); b \neq 0\end{aligned} \tag{42}$$

Consequently, the model of the nonlinear platform could now be written in terms of the linearising variable as

$$\begin{aligned}\theta_1 &= x_1 \\ \theta_2 &= \dot{x}_1 \\ \theta_3 &= \ddot{x}_1 \\ \theta_s - \theta_m &= \tan^{-1}\left\{\frac{1}{2bK_FDLI_RR_F}(\dddot{x}_1 + a_3\ddot{x}_1 + a_2\dot{x}_1 + a_1x_1)\right\}; b \neq 0\end{aligned} \tag{43}$$

Let,

$$\dot{x}_3 = v \tag{44}$$

Then

$$\begin{aligned}\dot{x}_1 &= x_2 \\ \dot{x}_2 &= x_3 \\ \dot{x}_3 &= -K_I(x_1 - x_1^*) - K_P(x_2 - x_2^*) - K_D(x_3 - x_3^*) = v(t)\end{aligned} \tag{45}$$

where x_1^*, x_2^*, x_3^* are the respective steady states of x_1, x_2, x_3 and

$$v = -a_1 x_1 - a_2 x_2 - a_3 x_3 + 2K_F K_1 I_R DLR_F bK_F \tan(\theta_s - \theta_m) \tag{46}$$

The nonlinear error measurements could now be written as:

$$\begin{aligned} \mu &= \theta_s - \theta_m = \tan^{-1}\left\{\frac{(\rho+\sigma)}{2bK_F K_1 LI_R R_F}\right\} \\ \rho &= -K_I(x_1 - x_1^*) - K_P(x_2 - x_2^*) - K_D(x_3 - x_3^*) \\ \sigma &= a_1 x_1 + a_2 x_2 + a_3 x_3 \end{aligned} \tag{47}$$

5.5.4 Tuning of the parameters of the nonlinear controller

For the evaluation of the v in equation (45), the controller parameters, K_I, K_P, K_D are chosen such that the stability of the linear system

$$\dot{x}_3 = -K_I(x_1 - x_1^*) - K_P(x_2 - x_2^*) - K_D(x_3 - x_3^*) \tag{48}$$

is guaranteed.
Now, define the error between the states and their references in the following manner:

$$\begin{aligned} \dot{x}_3(t) &= \dddot{e}(t) \\ x_3(t) - x_3^*(t) &= \ddot{e}(t) \\ x_2(t) - x_2^*(t) &= \dot{e}(t) \\ x_1(t) - x_1^*(t) &= e(t) \end{aligned} \tag{49}$$

And recast equation (48) in the form of equation (50):

$$(s^3 + K_D s^2 + K_P s + K_I)E(s) = 0 \tag{50}$$

Thus, select the tuning parameters K_I, K_P, K_D to ensure the asymptotic elimination of the error, such that.

$$\begin{aligned} \dot{x}_3(\infty) &\to 0 \\ x_3(\infty) &\to x_3^*(\infty) \\ x_2(\infty) &\to x_2^*(\infty) \\ x_1(\infty) &\to x_1^*(\infty) \end{aligned} \tag{51}$$

Here we proceed to chose K_I, K_P, K_D applying the Routh-Hurtwits criterion to the equivalent s polynomial:

$$s^3 + K_D s^2 + K_P s + K_I = 0 \tag{52}$$

Where

The nonlinear controller given by (43)-(47) shall be simulated and its impact on the dynamics of the platform compared with that of the linear controller.

5.6 Comparative simulation of the impact of nonlinear controller

Simulations comparing the performance of the platform under the impact of the feedback-linearised controller, with that under the impact of the pole-cancellation controller are shown in Figure 20 to Figure 22. The nonlinear system brings the system to rest within two seconds, as would the reference linear model. Overshoots are virtually eliminated in the dynamics of θ_m. Whereas the pole-cancellation strategy also brought the system to rest within two seconds, the accelerations observed in other system variables were very high. Overshoots remained significant. The nonlinear controller being reported in this paper achieves the same settling time and eliminates overshoots without causing excessive accelerations.

6. Conclusions and recommendations

6.1 Conclusions

The high overshoots associated with the dynamic response of the pole-cancellation controller could significantly add to the hardware costs of the tracking systems. Moreover, parameter uncertainty/variations could significantly compromise the performance of the platform under linear control. Feedback-linearised control of the platform yield exact linearization of platform dynamics, by feedback, without any approximations. It is demonstrated that this exact linearization leads to a better performance of the platform under the action of the feedback-linearised controller.

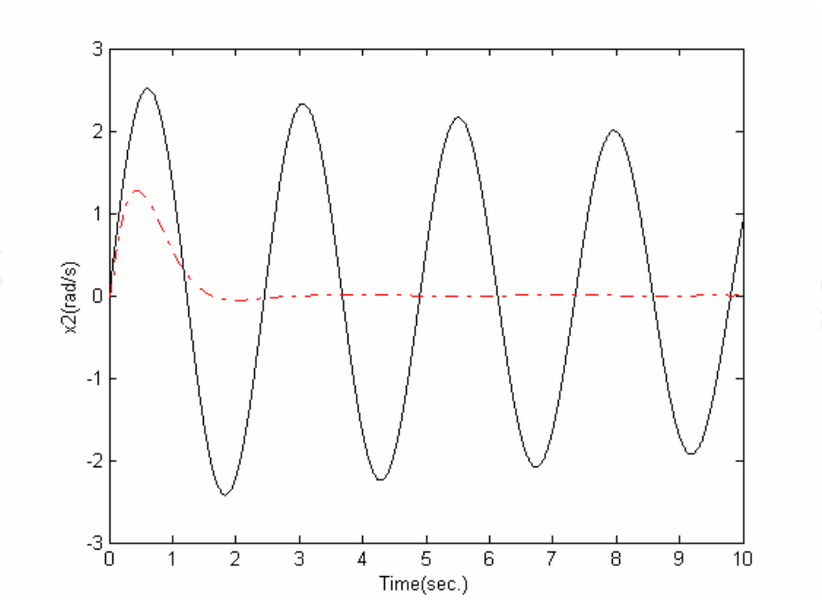

Fig. 20. Platform position under nonlinear control (_._) and linear control (---)

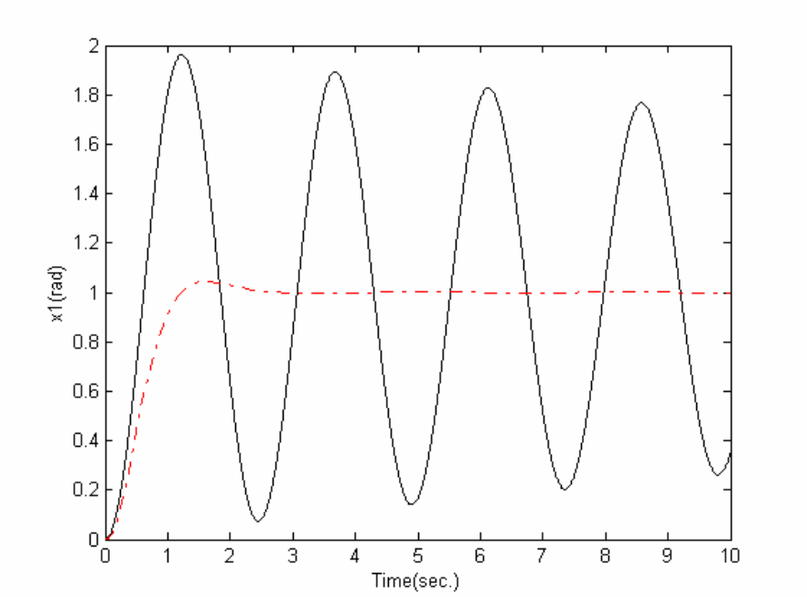

Fig. 21. Platform velocity under nonlinear control (_._) and linear control (----)

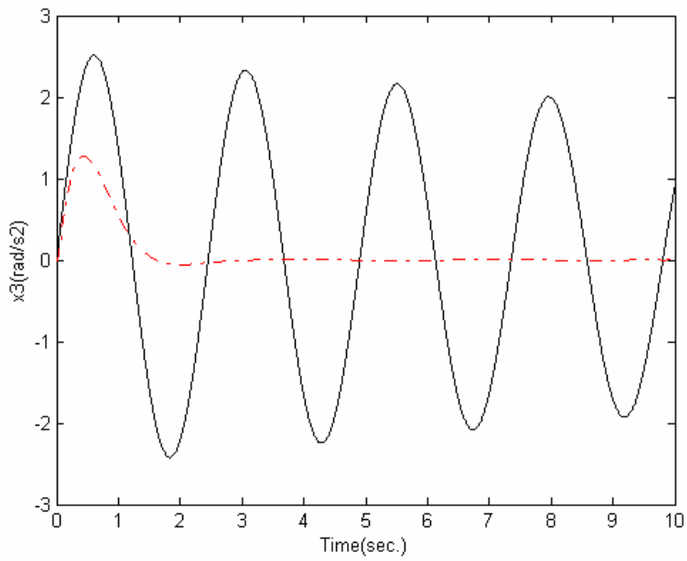

Fig. 22. Platform acceleration under nonlinear control (_._._) and linear control (----)

6.2 Recommendation for further studies

Further research directions here would consider the methods and costs of controller implementation. The feedback-linearised control strategy leads to a nonlinear controller

whose structure is more complex than that of the linear pole-cancellation controller. It is recommended to explore neural networks for the implementation of the nonlinear controller. The basic structure of the solar tracker system is linear. The subsequent nonlinearity in the system is due to the measurement. It is recommended to further explore the use of a linear sensor or even sensor-less tracking strategies to simplify controller design.

7. References

Anderson, G. O. & Abkenari, M. H., (1990) Application of solar energy technology in Botswana. *Proceeding of IASTED Int. Conf. on Power and Energy Systems*. Las Vegas, Nevada, 1999, 141-150.

Agee, J. T., Masupe, S, Jeffrey, M. & Jimoh A. A.Enhancing the Output Characteristics of a Photovoltaic Position Snesor Using a feed-Forward Neural network, Advance Materials Research, Vol. 62-62, pp. 506-511. 2009

J. T. Agee, A. A. Jimoh (2007) Feedback linearised Control of a Solar Power Platform. IEEE Africon 2007. Namibia.

J. T. Agee, M. de Lazzer an M. K. Yanev, "A Pole cancellation strategy for stabilising a 3KW solar power platform. *Int. Conf. Power and Energy Systems(EuroPES 2006*), Rhodes, Greece. June 26-28.

J. T. Agee, S. Obok-Opok and M. de lazzer, "Solar tracker technologies: market trends and field applications. *Int. Conf. on Eng. Resaerch and Devlopemnt: Impact on Industries*. 5-7th September, 2006.

Alternative Energy Store, 300W Shott Solar panel specifications. http://shop.altenergy store.com, 2005.

Archer, M. and Hill, R. (2001), Clean Electricity from Photovoltaics Botswana Power. http://www.wn.com /s/ Botswana power . 2004.

Southern Africa and the Southern African Development Community. http://www. eia.doe.gov /meu/cabs/sadc .hmtl. 2005.

Consultancy on Identifying and Overcoming Barriers to Widespread Adoption of Renewable Energy – Based Rural Electrification in Botswana: *Final report.* 2003.Customer Tips http://www.bpc.bw 10-2005

Daily energy consumption http://www.epsic.ch/pagesperso/ schneiderd/ Apelm /Sources/Solaire.htm 10-2005

De Lazzer, M. (2005). A positioning System for an Array of Solar Panels. Unpublished M.Sc Thesis University of Botswana.

Geche, J. & Irvine J. (1996). Photovoltaic Lighting in Rural Botswana: A Pilot Project. Renewable Energy for Development, Vol. 9, No. 2, pp. http://www.sei.se/red /red9609e.html 21st July, 2009

B. C. Kuo & F. Golnaraghi, *Automatic Control Systems* (eight edition, John Wiley and Sons, Inc., 2003).

Lasschuit, P, Westra, C. & van Roekel G., (xxxx). Financial Suatainability of PV Implementation in Swaziland. http://roo.undp.org/gef/solarpv/docs/bgmaterial /Misc%20PV%20Papers/ECN%20-%20Financial%20sustainability%20of%20PV %20implementation %20in%20Swaziland.pdf. 21st July, 2009

N. Matenge & V. Masilo, *Feasibility Study of Botswana Electricity Generation*(HND Project, *Power Point Presentation*, University of Botswana, 2004).

Mogotsi, B. (2002). Energy and Sustainable Development in Botswana. Sustainable Energy Watch Report. HELIO-Botswana. Helio International. http://www.helio-international.org /reports/2002/botswana.cfm. 21st July, 2009

Nelso, J (2003), The Physics of Solar Cells. Barnes and Noble.

N. S. Norman, *Control Systems Engineering* (John Willey and Sons, Inc. USA , 2004).

Shell SQ 80W solar panel specifications. http://www.shell.com, 2005.

TRACSTAR (Small Power systems) Solar Tracking for Architects Source: http://www. pacificsites.com/ sps/trackforarc.html, 2006.

IntechOpen

Solar Energy

Edited by Radu D Rugescu

ISBN 978-953-307-052-0
Hard cover, 432 pages
Publisher InTech
Published online 01, February, 2010
Published in print edition February, 2010

The present “Solar Energy” science book hopefully opens a series of other first-hand texts in new technologies with practical impact and subsequent interest. They might include the ecological combustion of fossil fuels, space technology in the benefit of local and remote communities, new trends in the development of secure Internet Communications on an interplanetary scale, new breakthroughs in the propulsion technology and others. The editors will be pleased to see that the present book is open to debate and they will wait for the readers’ reaction with great interest. Critics and proposals will be equally welcomed.

How to reference

In order to correctly reference this scholarly work, feel free to copy and paste the following:

John T. Agee and Adisa A. Jimoh (2010). Control of a 3KW Polar-Axis Solar Power Platform with Nonlinear Measurements, Solar Energy, Radu D Rugescu (Ed.), ISBN: 978-953-307-052-0, InTech, Available from: http://www.intechopen.com/books/solar-energy/control-of-a-3kw-polar-axis-solar-power-platform-with-nonlinear-measurements

INTECH
open science | open minds

InTech Europe
University Campus STeP Ri
Slavka Krautzeka 83/A
51000 Rijeka, Croatia
Phone: +385 (51) 770 447
Fax: +385 (51) 686 166
www.intechopen.com

InTech China
Unit 405, Office Block, Hotel Equatorial Shanghai
No.65, Yan An Road (West), Shanghai, 200040, China
中国上海市延安西路65号上海国际贵都大饭店办公楼405单元
Phone: +86-21-62489820
Fax: +86-21-62489821

© 2010 The Author(s). Licensee IntechOpen. This chapter is distributed under the terms of the Creative Commons Attribution-NonCommercial-ShareAlike-3.0 License, which permits use, distribution and reproduction for non-commercial purposes, provided the original is properly cited and derivative works building on this content are distributed under the same license.

IntechOpen

IntechOpen